Interfacial Effects on Nanoconfined Diffusive Mass Transport Regimes

A. Ziemys, M. Kojic, M. Milosevic, and M. Ferrari

Phys. Rev. Lett. **108**, 236102 — Published 6 June 2012

DOI: 10.1103/PhysRevLett.108.236102

Interfacial effects on nanoconfined diffusive mass transport regimes

A.Ziemys[1]*, M.Kojic[1,2], M.Milosevic[2], M.Ferrari[1]

* - corresponding author

[1] - The Methodist Hospital Research Institute, The Department of Nanomedicine, 6670 Bertner Ave., R7-116, Houston, TX 77030. [2] – University Metropolitan Belgrade - Bioengineering Research and Development Center BioIRC, Kragujevac Prvoslava Stojanovica 6, 3400 Kragujevac, Serbia

Keywords: diffusion, mass transport, non-Fickian, nanochannel, nanoconfinement.

Abstract

A hierarchical multiscale modeling approach, incorporating Molecular Dynamics and Finite Element techniques, was used to study parametrically diffusion regimes through nanoconfined fluid. Novel parameters which determine the character of the diffusion regime and diffusion kinetics within the nanoscale confined fluids were established by exploring diffusion where the interface effects at the solid surface are important. New diffusion transport characteristics are established when nanochannel confining dimension approaches 3-4 sizes of diffusing molecules, which also marks peripheries of the non-Fickian transport regime.

Confined nano- or micro-scale fluidic systems are found widely in natural geological formations (e.g. sedimentary rocks [1]) and biology (e.g. cellular pores [2]), or in devices containing nanochannels or nanopores. Many nanofluidic technologies are implemented in biomedical applications [3-5], where mass exchange is the governing process. In nano-confined structures solid surfaces can alter both fluid and solute properties at the interface [6, 7], resulting in the dominance of surface effects over volumetric material properties. In diffusive mass transport of a solute through a fluid, both the fluid and solute may interact with the solid surfaces [8, 9] bounding the diffusion domain that may alter diffusion characteristics near the fluid-solid interface [10, 11]. When the diffusive domain is confined by solid surfaces of small lengths, like in nanochannels or nanopores, interface interactions may profoundly change diffusion resulting in deviations from Fick's law. Although non-Fickian diffusion has been discussed for decades [12, 13] and nanochannel structures appeared available for studies in the mid-nineties [14, 15], the causes of non-classical diffusion transport regimes are still not fully understood.

In this Letter, we apply a hierarchical multiscale modeling approach to elucidate the impact of interface and nanochannel structure effects on diffusion regimes through nanoconfined fluid. Traditional continuum approaches for modeling nanoconfined diffusion are inadequate, since they omit interfacial effects. To overcome the limitations of classical diffusion modeling and prediction, we have recently developed a hierarchical computational approach that bridges nanoscale interface effects with a discretized continuum Finite Element (FE) method [16, 17]. This new computational approach relies on a diffusivity scaling function derived from a diffusion coefficient profile at the interface of the nanochannel with the use of Molecular

Dynamics (MD) simulations. The diffusivity scaling function *S(c,h)* was evaluated for glucose as a model for neutral small molecules [18] (Figure 1A). The function *S(c,h)* rescales an experimental bulk diffusion coefficient D_B so that the effective diffusivity depends on the local concentration *c* and the proximity to surface *h*: $D(c,h)=S(c,h)\cdot D_B(c)$. This methodology was incorporated in the FE method [19], used to model nanochannels, and it was quantitatively and qualitatively validated against experiments [16]. The basic mass balance equation, which also includes Fick's law

$$J = -D\nabla c \qquad (1)$$

is

$$-\frac{\partial c}{\partial t} + \frac{\partial}{\partial x_i}\left(D\frac{\partial c}{\partial x_i}\right) + q = 0 \qquad (2)$$

where *J* is the mass flux, $c(x_i,t)$ is concentration at a spatial point with coordinates x_i and at a time *t*; *D* depends in general on x_i and on *c*; $q(x_i,t)$ is a source term, and summation over the repeated index is implied ($i=1,2,3$). By using a standard Galerkin procedure, this nonlinear differential equation is transformed into a linear incremental-iterative system of balance equations for a finite element assemblage [20].

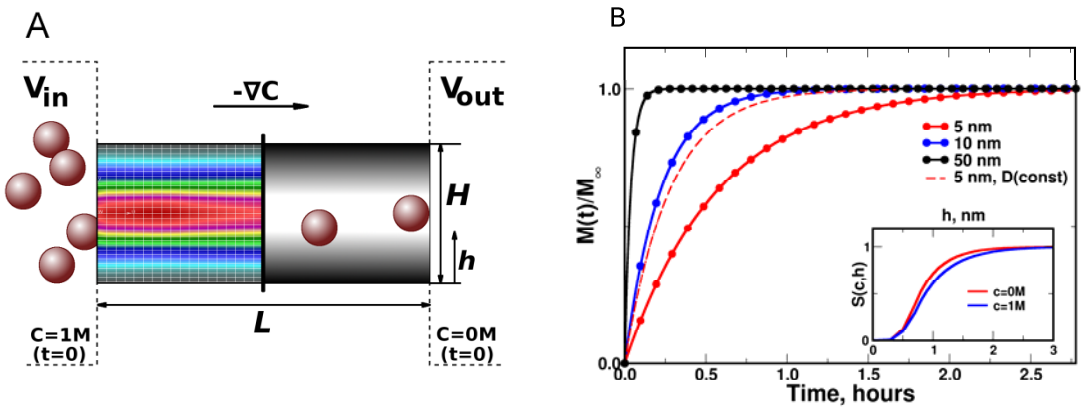

Figure 1. Nanochannel model. A) The model consists of nanochannel with length *L* and height *H* connecting two reservoirs (V_{in} and V_{out}) with different concentrations *c* at time *t*=0. The left side of the nanochannel depicts representative diffusive flux field that depends on the proximity to surface *h*; the gray gradient on the right side depicts decreasing diffusivity by approaching surface, and this decrease is modeled by using *S(c,h)*. B) Calculated cumulative mass release $M(t)/M_\infty$ through 1 µm long nanochannel with three nanochannel heights using *D(c,h)*. $M(t)/M_\infty$ of 5 nm nanochannel assuming *D(const)* (red dashed line) is presented for comparison with the case *D(c,h)*. The inset shows the scaling the function S(c,h) for 0 and 1 M solutions used in the calculations.

We have studied diffusion in nanochannels with 0.5, 1, 3, 10 µm lengths (*L*) and 1, 3, 5, 10, 20, 50 nm heights (*H*) with fixed width of 1 µm as depicted in Figure 1A; these geometries covered characteristic dimensions of representative nanofluidic structures as reviewed in [21]. The nanochannel connects donor (inlet) and acceptor (outlet) reservoirs with $1 \cdot 10^{-6}$ µL volume each. At time zero, the donor reservoir was filled with 1 M solution, while the other reservoir

had zero concentration. The cumulative mass release (Figure 1B) by passive diffusion was calculated following the approach outlined in [16]. The diffusivity was treated by three scenarios: *D(const)* - *D* is constant as in an ideal solution; *D(c)* - *D* is a function of concentration c; *D(c,h)* - *D* is the function of concentration *c* and the proximity to solid wall *h*. We used a representative *D* value for small molecules in water, where *D* was $1.0 \cdot 10^{-6}$ cm^2/s as for infinite dilution. In *D(c)* and *D(c,h)* cases, diffusivity linearly changed from $1.0 \cdot 10^{-6}$ cm^2/s at zero concentration to $0.5 \cdot 10^{-6}$ cm^2/s at 1 M; and scaling functions were used according to graphs in the inset of Figure 1B.

A cumulative mass release was calculated until uniform (equal to zero within a numerical tolerance) concentration was reached, with no further mass release as shown in Figure 1B. We found that all release profiles showed exponential-like profiles, but with different stretch: the stretch of the release curve was increasing a) in the order of diffusivity *D(const)*<*D(c)*<D*(c,h)*, and b) with increasing nanochannel length or decreasing height. By comparing mass release curves for 5 nm nanochannel with *D(const)* and *D(c,h)* in Figure 1B, it can be seen that the inclusion of nanochannel interface effects can have a significant impact on release kinetics. Here, we note that classical analytical solution exists for equation (2) for *D(const).* Then, in the case of 1D diffusion, variable decomposition can be used to solve the balance equation

$$\frac{\partial c}{\partial t} = D \frac{\partial^2 c}{\partial x^2} \qquad (3)$$

The analytical solution leads to a mass release in a form of the saturated exponential [22], like:

$$M(t)/M_\infty = 1 - \exp(-\lambda t) \qquad (4)$$

where M_∞ is the proportionality constant or the mass released at infinite time; *M(t)* is the cumulative released mass at time *t* and λ is the exponent describing the kinetics of the diffusion. In general, there is no analytical solution in a closed form in the D(c) case, as well as in more complex case of *D(c,h)*. Both *D(c)* and *D(c,h)* are highly dependent on the nature of material properties [8], since different molecular interactions will lead to different *D(c)* and *S(c,h)*.

As all solutions rely on the balance equation (2) leading to a mass release form (4) for *D(const)*, we used equation (4) to characterize all numerical solutions by fitting the value of λ. We have analyzed λ values in terms of the ratio $L/H=\alpha$. Since *L* and *H* have direct relations to the gradient and cross-sectional (flux) area of nanochannel, respectively, the results of our analysis may be further generalized to other nanofluidic geometries and volumes.

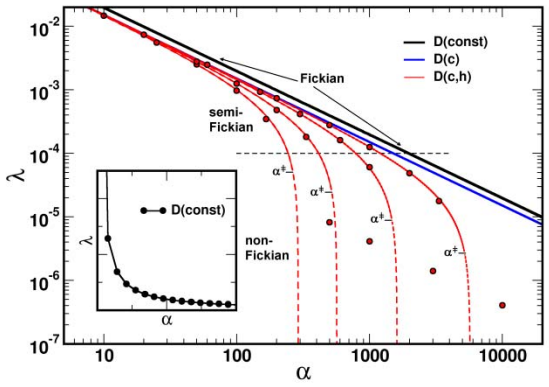

Figure 2. The dependence of λ on the length to height ratio $\alpha=L/H$ of nanochannel in a double logarithmic scale. Solid curves represent fitted lines using eq. (5). The calculated points $\lambda(\alpha)$ for *D(c,h)* are marked by red dots, while the data points of *D(const)* and *D(c)* lie on straight fitting lines and are omitted for visual purpose. The case *D(c,h)* separates $\lambda(\alpha)$ into a family of

curves, so that the same λ value can be obtained from different α as marked by black dashed line crossing *D(c,h)* curves. A ten-fold decrease of λ (on *D(c,h)* curves) from *D(c)* line establishes $\alpha^{\ddagger}$ values on *D(c,h)* curves, beyond which non-Fickian transport is observed (dashed lines). The inset contains representative hyperbolic $\lambda(\alpha)$ curve in linear coordinates for *D(const)*.

We have introduced a function $\lambda(\alpha)$:

$$\lambda(\alpha) = A + B/\alpha \qquad (5)$$

with arbitrary coefficients *A* and *B* to characterize the calculated mass release according to Equation (4). The λ values were evaluated for various combinations of *L* and *H* taking diffusivity as *D(const)*, *D(c)* and *D(c,h)* and plotted against α in Figure 2. We further analyze the relation $\lambda(\alpha)$ for computed mass release curves fitted by equation (4) for the three assumptions regarding the diffusivity. In the cases of *D(const)* and *D(c)*, the $\lambda(\alpha)$ function is represented by straight lines in the double logarithmic scale, Fig. 2, using equation (5) with A=0. Both cases correspond to a free diffusion regime with the mass release kinetics according to equation (4), which will be called as Fickian through the manuscript. The diffusivity dependence on concentration does not change the mechanism of diffusion, it only leads to a reduced transport kinetics: the line for D(c) is below the line *D(const)*, λ is smaller (for the same α) and consequently the mass release is slower. These straight lines, i.e. the linear functions $\lambda(\alpha)$ (in the double logarithmic scale representation), also demonstrate that for a given geometric ratio α=L/H there is a unique value of λ and a unique transport kinetics of the nanochannel within the free diffusion regime.

However, the inclusion of interface effects with *D(c,h)* reveals qualitative and quantitative difference of *λ(α)* with respect to free diffusion. The *λ* values from *D(c,h)* overlap with *D(c)* case at small *α*, but start to deviate from *D(c)* scenario forming a *λ(α)* family of curves corresponding to specific values of *L* (Figure 2). By inspecting these *λ(α)* curves, it is taken that when the difference between the *λ* value at the curve *D(c)* and on the *λ(α)* curve is ten-fold, the onset of non-Fickian occurs and the corresponding value $\alpha=\alpha^{\ddagger}$ is considered critical. We have that each *λ(α)* curve obeys Equation (5) for *α* much below $\alpha^{\ddagger}$, then the difference with respect to the straight line starts to increase in the regime termed as semi-Fickian (see Figure 2). Finally, for *α* above $\alpha^{\ddagger}$ the difference is further increased and the diffusion regime becomes non-Fickian, where Equation (5) is no longer applicable. Figure 3 depicts *λ(α)* using *D(c,h)* for three systems with different inlet and outlet reservoirs: 1 µL / 1 µL, 5 µL / 1 µL, and 5 µL / 5 µL. The *λ(α)* curves show that reservoir volumes affect diffusion kinetics. However, no matter what volume we may choose, the critical value $\alpha^{\ddagger}$ remains the same, therefore diffusion transport regime is only dictated by nanochannel properties: *H*, *L* and surface physic-chemistry, which is incorporated in our computational method with diffusivity scaling functions.

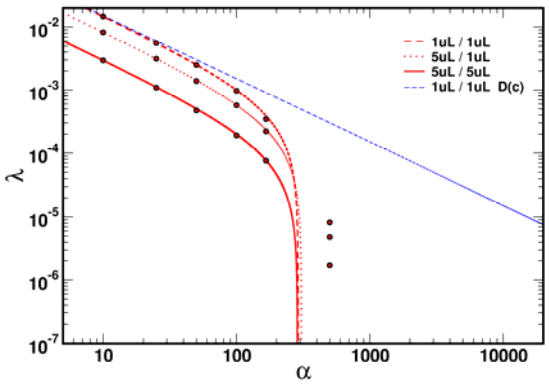

Figure 3. Dependence $\lambda(\alpha)$ for three systems having nanochannel with L = 0.5 μm and different inlet and outlet reservoir volumes using *D(c,h)*: 1 μL / 1 μL, 5 μL / 1 μL, and 5 μL / 5 μL. Critical value $\alpha^{\ddagger}$ is the same for all reservoir volumes, hence $\alpha^{\ddagger}$ depends on the nanochannel properties. *D(c)* system having both reservoirs volumes of 1 μL is given for visual comparison.

By the incorporation of interface effects to diffusivity, calculated mass release is characterized by the family of $\lambda(\alpha)$ curves, where each curve corresponds to a specific length *L*. Identical λ values may be found for different α, meaning that the same diffusive mass transport kinetics occurs in nanochannels with different geometries. That is illustrated by black dashed line in Figure 2 that crosses different $\lambda(\alpha)$ curves. Figure 4 shows two mass release curves that completely overlap ($\lambda = 5 \cdot 10^{-4}$ for both curves), although this mass release is computed for nanochannels having two different α: *L/H* = 0.5μm/3.4nm and 1.0μm/5nm. This finding represents a new phenomenon for the diffusion in nanochannels: the same diffusion mass transport kinetics (the same λ) can occur for different geometric parameters *L* and *H* due to surface interaction effects in case when α is larger than the critical value $\alpha^{\ddagger}$, *i.e.* where diffusion is semi-Fickian. Therefore, surface interactions play a role of an additional parameter for confined diffusion at nanoscale.

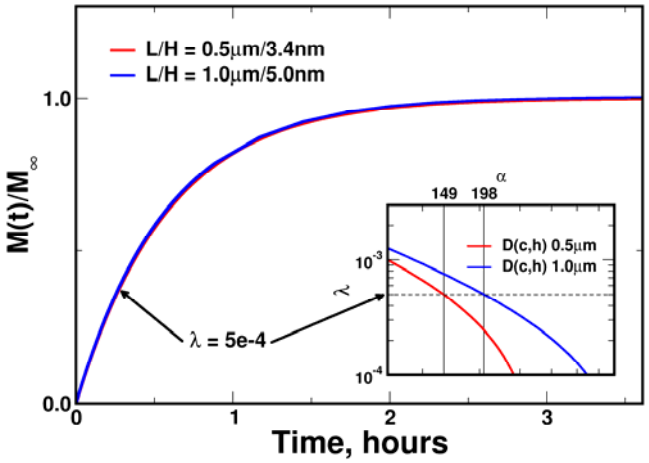

Figure 4. Diffusion in a semi-Fickian regime. Practically the same diffusion kinetics ($\lambda = 5 \cdot 10^{-4}$ in Eq.4; dashed line in the inset) occurs through nanochannels having different α (*L/H* = 0.5μm/3.4nm and 1.0μm/5nm). The inset shows characteristic portions of $\lambda(\alpha)$ profiles for *L* = 0.5 and 1 μm.

From the analysis of Figures 2-4, it follows that Equation (1) will be violated by the breakdown of Fickian diffusion regime at small nanopores or nanochannels, when diffusing molecule size becomes comparable to a confining dimension (*i.e.* nanochannel height *H*). With α values close to or larger than $\alpha^{\ddagger}$ we reach the diffusion regime where the classical theory cannot handle the diffusion process. For nanochannels with *L* equal to 0.5, 1, 3 and 10 μm the calculated $\alpha^{\ddagger}$ are 261, 510, 1451 and 5153. Using $\alpha^{\ddagger}$ we can predict dimensions of nanochannels, where Fickian diffusion regime is breaking down. With $\alpha^{\ddagger} = L/H$ and known *L*, we found that the critical height for slit-like nanochannel is approximately 1.9 nm. This value converges from all four investigated nanochannel lengths *L*, modeled with a use of the same

diffusion scaling function. Since the glucose molecule is of size of 0.5 nm, we obtained that the critical height of nanochannel is approximately 3-4 molecular sizes. In experimental studies of different molecules diffusion through different size of nanochannels [23, 24] it was found that the non-Fickian diffusion regime occurs when the ratio of the nanochannel height to the molecular size is in the range found by our calculations. Other experiments with human serum albumin (HSA) and human growth hormone release (hGH) through polymer/gold nanopores support our model [25]: HSA showed Fickian release through 200 nm pore and zero-order release through 15 nm pore, while hGH diffusion was Fickian through 15 nm pore and zero-order released through 6 nm pore. HSA and hGH dimensions are approximately 8 and 4 nm leading to pore/size ratios 1:25 and 1:4 for free diffusion, and 1:2 and 1:1.5 ratios for zero-order release. These findings also confirm that our model agrees well with experimental observations indicating that $\alpha^{\ddagger}$ could discriminate well Fickian and non-Fickian regimes.

Our model and analysis revealed that the inclusion of interface effects on diffusivity can have a deep impact on prediction of mass transport at nanoscale. Besides more realistic description of diffusive mass transport, we have found deterministic parameters to establish diffusion regimes and to predict new nanofluidic transport effects. By using the dependence $\lambda(\alpha)$, where $\alpha=L/H$ is the ratio of the channel length L and height H, we determined the conditions for the Fickian or non-Fickian diffusion regime to occur within nanochannels. The $\alpha=\alpha^{\ddagger}$ serves as a critical parameter, which demarks diffusion mechanisms: $\alpha < \alpha^{\ddagger}$ follows the Fickian-like release kinetics, while for $\alpha \approx \alpha^{\ddagger}$ and $\alpha > \alpha^{\ddagger}$ the kinetics is non-Fickian. Our results suggest a new nanofluidic diffusion phenomenon: the same transport kinetics can be achieved by different nanochannel geometries. This opens possibilities to rationalize kinetics of diffusive mass

transport through nanofluidic devices tailoring transport rates and regimes. Our parametric study offers a new insight into the diffusive mass transport through nanoconfined structures and establishes relations among geometry, interface effects and mass transport kinetics. Although the presented approach relies on simplifications of the diffusion transport problem in nanoconfinement and additional studies might be required for more complex systems, the introduced novel parametric study of diffusion at nanoscale may have an impact on nanotechnology and design of biomedical devices.

The authors acknowledge the Texas Advanced Computing Center (TACC) at The University of Texas at Austin for providing HPC resources that have contributed to the research results reported within this paper. This project has been partially supported with federal funds from NASA under the contracts NNX08AW91G and Alliance of NanoHealth (ANH), and from Ministry of Education and Science of Serbia, grant OI 174028.

References

1. T. B. Boving and P. Grathwohl, J. Contam. Hydrol. **53** (1-2), 85-100 (2001).
2. F. Alber, S. Dokudovskaya, L. M. Veenhoff, W. Zhang, J. Kipper, D. Devos, A. Suprapto, O. Karni-Schmidt, R. Williams and B. T. Chait, Nature **450** (7170), 683-694 (2007).
3. J. Mannion and H. Craighead, Biopolymers **85** (2), 131-143 (2007).
4. J. Han, J. Fu and R. Schoch, Lab Chip **8** (1), 23 (2008).

5. J. Sakamoto, A. van de Ven, B. Godin, E. Blanco, R. Serda, A. Grattoni, A. Ziemys, A. Bouamrani, T. Hu, S. Ranganathan, E. Derosa, J. Martinez, C. Smid, R. Buchanan, S. Lee, S. Srinivasan, A. Meyn, E. Tasciotti, X. Liu, P. Decuzzi and M. Ferrari, Pharmacol. Res. **62** (2), 57–89 (2010).
6. M. Hosoda, K. Sakai and K. Takagi, Phys. Rev. E **58** (5), 6275-6280 (1998).
7. D. Topgaard and O. Söderman, Langmuir **17** (9), 2694-2702 (2001).
8. S. K. Parida, S. Dash, S. Patel and B. Mishra, Adv. Colloid Interface Sci. **121** (1-3), 77-110 (2006).
9. J. Israelachvili and H. Wennerström, Nature (379), 219 - 225 (1996).
10. P. Holmqvist, J. Dhont and P. Lang, Phys. Rev. E **74** (2), 21402-21407 (2006).
11. M. Reedijk, J. Arsic, F. Hollander, S. De Vries and E. Vlieg, Phys. Rev. Lett. **90** (6), 66103 (2003).
12. O. Bénichou, C. Chevalier, J. Klafter, B. Meyer and R. Voituriez, Nature Chem. **2** (6), 472-477 (2010).
13. J. Crank and G. Park, Transactions of the Faraday Society **47**, 1072-1084 (1951).
14. G. Hornyak, K. Phani, D. Kunkel, V. Menon and C. Martin, Nanostructured Materials **6** (5-8), 839-842 (1995).
15. T. A. Desai, D. J. Hansford, L. Kulinsky, A. H. Nashat, G. Rasi, J. Tu, Y. Wang, M. Zhang and M. Ferrari, Biomed. Microdev. **2** (1), 11-40 (1999).
16. A. Ziemys, M. Kojic, M. Milosevic, N. Kojic, F. Hussain, M. Ferrari and A. Grattoni, J. Comput. Phys. **230** (14), 5722–5731 (2011).

17. M. Kojic, M. Milosevic, N. Kojic, M. Ferrari and A. Ziemys, Journal of the Serbian Society for Computational Mechanics/Vol **5** (1), 104-118 (2011).

18. A. Ziemys, A. Grattoni, D. Fine, F. Hussain and M. Ferrari, The Journal of Physical Chemistry B **114** (34), 11117–11126 (2010).

19. N. Kojic, A. Kojic and M. Kojic, Communications in Numerical Methods in Engineering **22** (9), 1003-1013 (2006).

20. M. Kojic, N. Filipovic, B. Stojanovic and N. Kojic, *Computer Modeling in Bioengineering: Theoretical background, examples and software*. (John Wiley & Sons, 2008).

21. D. Mijatovic, J. Eijkel and A. Van Den Berg, Lab Chip **5** (5), 492-500 (2005).

22. J. Crank, *The mathematics of diffusion, 2nd edn. Clarendon*. (Oxford, 1975).

23. D. Fine, A. Grattoni, S. Hosali, A. Ziemys, E. De Rosa, J. Gill, R. Medema, L. Hudson, M. Kojic and M. Milosevic, Lab Chip **10** (22), 3074-3083 (2010).

24. A. Grattoni, H. Shen, D. Fine, A. Ziemys, J. Gill, L. Hudson, S. Hosali, R. Goodall, X. Liu and M. Ferrari, Pharm. Res. **28** (2), 292-300 (2011).

25. S. Y. Yang, J. A. Yang, E. S. Kim, G. Jeon, E. J. Oh, K. Y. Choi, S. K. Hahn and J. K. Kim, ACS Nano **4** (7), 3817–3822 (2010).

Figure Captions

Figure 1. Nanochannel model. A) The model consists of nanochannel with length *L* and height *H* connecting two reservoirs (V_{in} and V_{out}) with different concentrations at time *t*=0. The left side of the nanochannel depicts representative diffusive flux field that depends on the proximity to surface *h*; the gray gradient on the right side depicts decreasing diffusivity by approaching surface, and this decrease is modeled by using *S(c,h)*. B) Calculated cumulative mass release $M(t)/M_\infty$ through 1 μm long nanochannel with three nanochannel heights using *D(c,h)*. $M(t)/M_\infty$ of 5 nm nanochannel assuming *D(const)* (red dashed line) is presented for comparison with the case *D(c,h)*. The inset shows the scaling the function S(c,h) for 0 and 1 M solutions used in the calculations.

Figure 2. The dependence of λ on the length to height ratio $\alpha=L/H$ of nanochannel in a double logarithmic scale. Solid curves represent fitted lines using eq. (5). Points $\lambda(\alpha)$ for *D(const)* and *D(c)* lie on straight lines and are omitted for visual purpose. The case *D(c,h)* separates $\lambda(\alpha)$ into a family of curves, so that the same λ value can be obtained from different α as marked by black dashed line crossing *D(c,h)* curves. A ten-fold decrease of λ (on *D(c,h)* curves) from *D(c)* line establishes $\alpha^{\ddagger}$ values on *D(c,h)* curves, beyond which non-Fickian transport is observed

(dashed lines). The inset contains representative hyperbolic *λ(α)* curve in linear coordinates for *D(const)*.

Figure 3. Dependence *λ(α)* for three systems having nanochannel with L = 0.5 μm and different inlet and outlet reservoir volumes using *D(c,h)*: 1 μL / 1 μL, 5 μL / 1 μL, and 5 μL / 5 μL. Critical value $\alpha^{\ddagger}$ is the same for all reservoir volumes, hence $\alpha^{\ddagger}$ depends on the nanochannel properties. *D(c)* system having both reservoirs volumes of 1 μL is given for visual comparison.

Figure 4. Diffusion in a semi-Fickian regime. Practically the same diffusion kinetics ($\lambda = 5 \cdot 10^{-4}$ in Eq.4; dashed line in the inset) occurs through nanochannels having different *α* (*L/H* = 0.5μm/3.4nm and 1.0μm/5nm). The inset shows characteristic portions of *λ(α)* profiles for *L* = 0.5 and 1 μm.

Figure 1 A

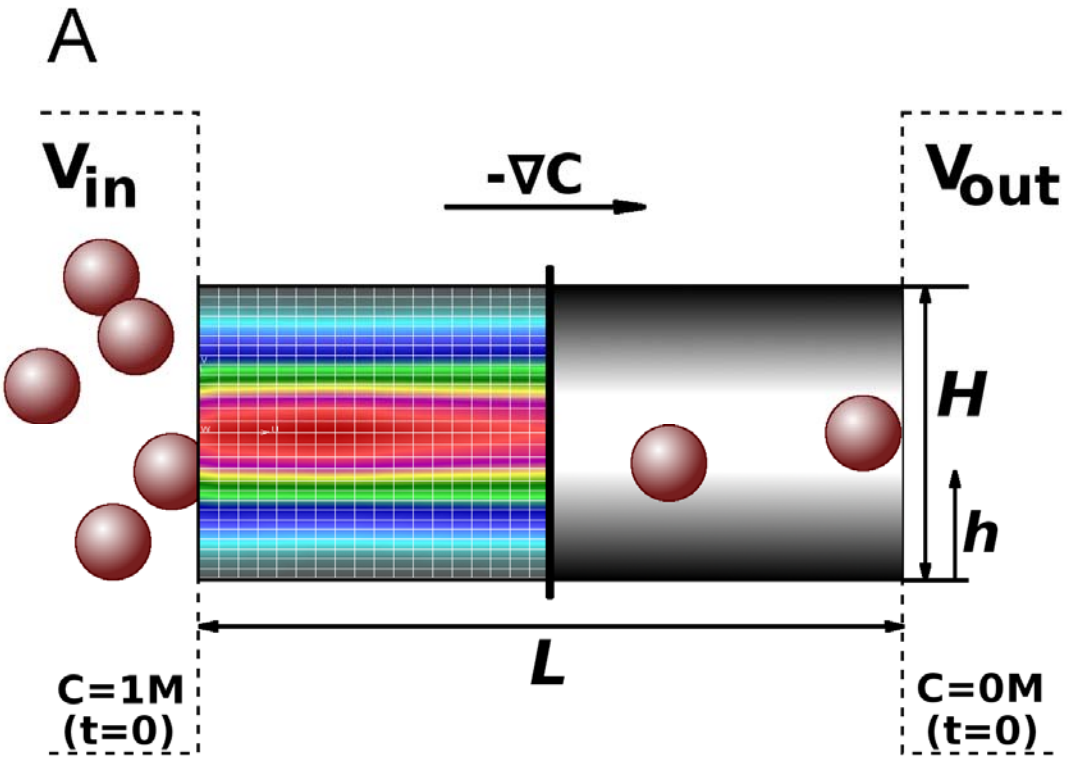

Figure 1 B

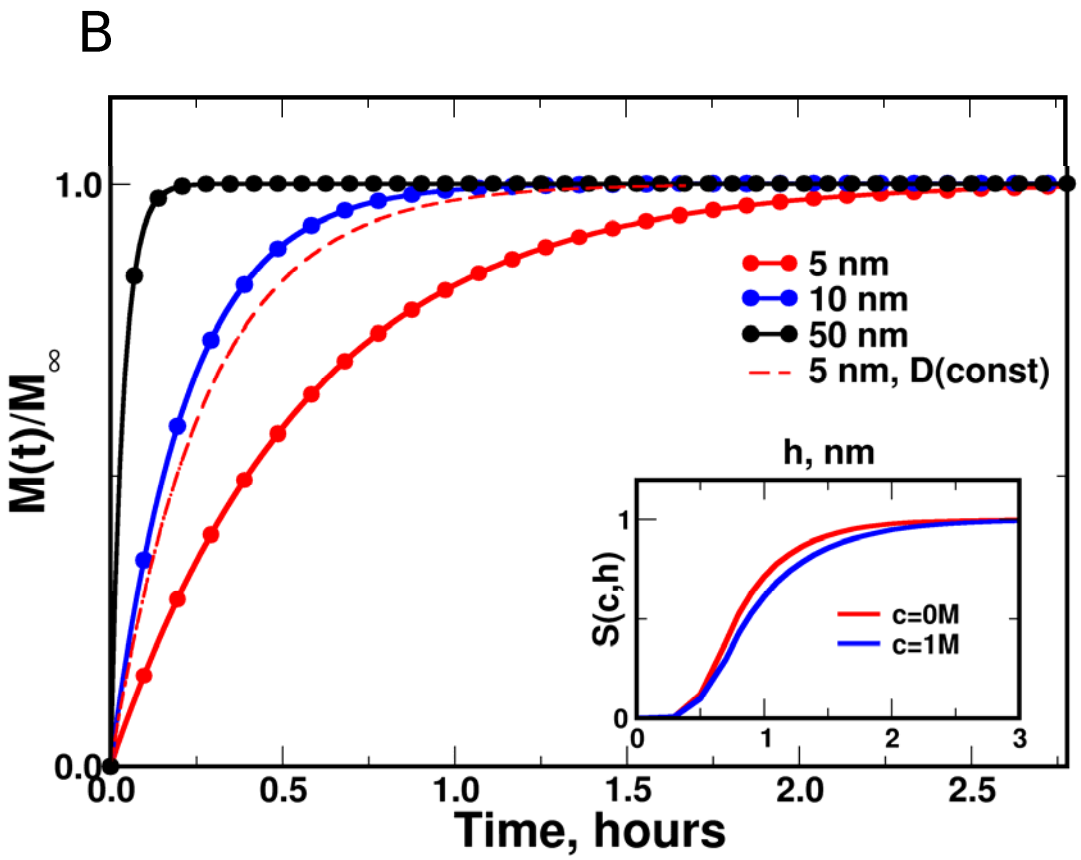
B
1.0
0.0
M(t)/M∞
0.0
0.5
1.0
1.5
2.0
2.5
Time, hours
5 nm
10 nm
50 nm
5 nm, D(const)
h, nm
S(c,h)
c=0M
c=1M
0
1
2
3

Figure 2

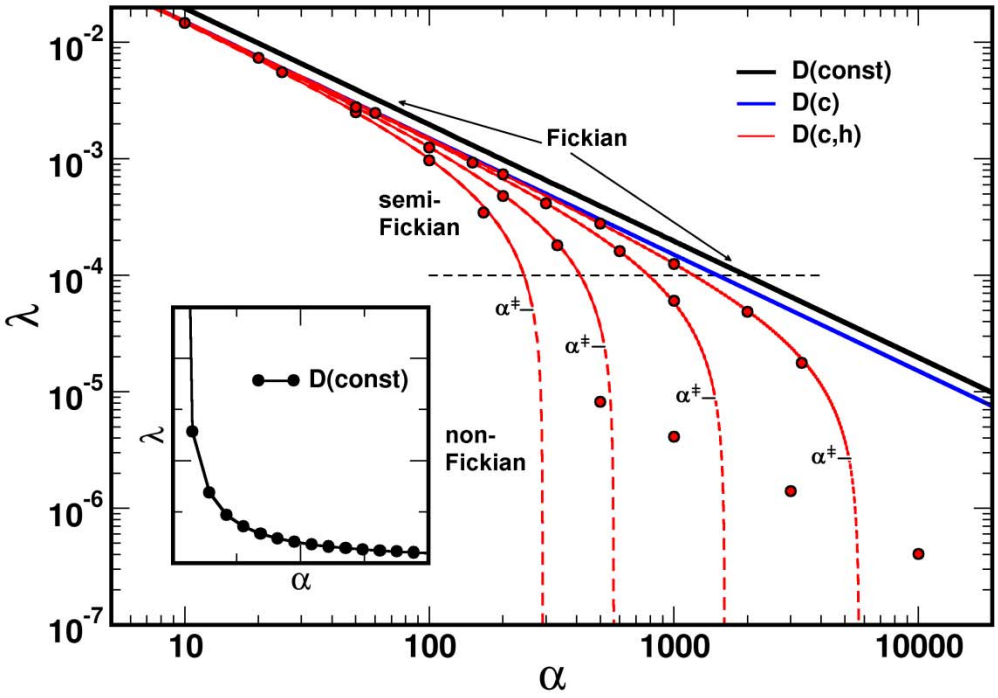
D(const)
D(c)
D(c,h)
Fickian
semi-
Fickian
non-
Fickian
α‡
λ
α
10
100
1000
10000
10^-2
10^-3
10^-4
10^-5
10^-6
10^-7

Figure 3

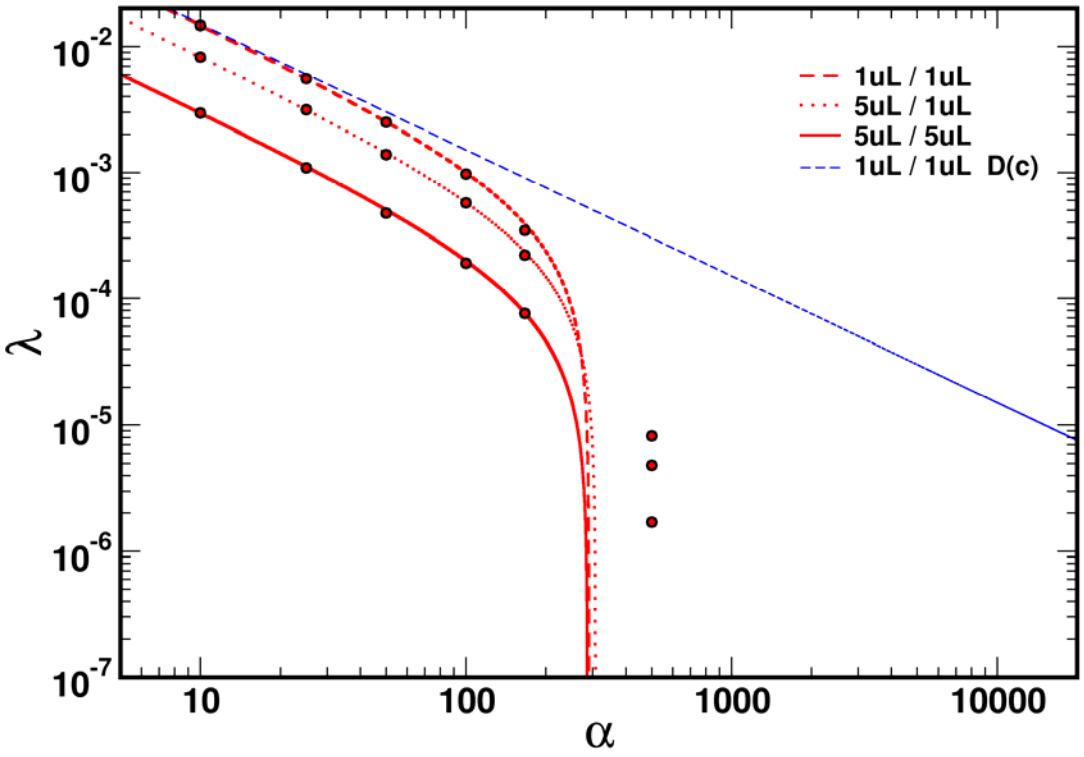
1uL / 1uL
5uL / 1uL
5uL / 5uL
1uL / 1uL D(c)
λ
α
10^-2
10^-3
10^-4
10^-5
10^-6
10^-7
10
100
1000
10000

Figure 4

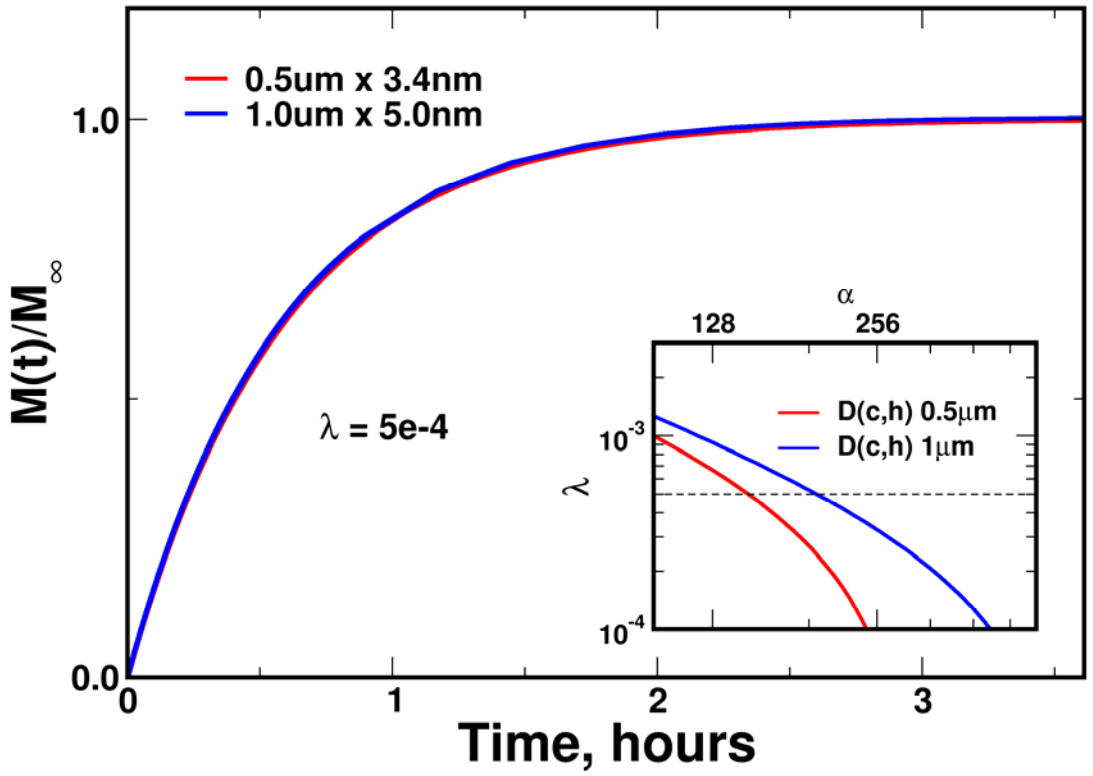
0.5um x 3.4nm
1.0um x 5.0nm
1.0
0.0
M(t)/M∞
λ = 5e-4
α
128
256
λ
10^-3
10^-4
D(c,h) 0.5μm
D(c,h) 1μm
0
1
2
3
Time, hours